A piezoelectric beam model with geometric, material and damping nonlinearities for energy harvesting

A piezoelectric beam model with geometric, material and damping nonlinearities for energy harvesting

Claudio D. Gatti[1,2], Mariano Febbo[3], Sebastián P. Machado[1,2] and Santiago M. Osinaga[1,2]

[1] Consejo Nacional de Investigaciones Científicas y Técnicas (CONICET), Argentina.
[2]Grupo de Investigación en Multifísica Aplicada (GIMAP), Universidad Tecnológica Nacional FRBB, 11 de Abril 461, 8000 Bahía Blanca, Argentina.
[3]Instituto de Física del Sur (IFISUR) and Departamento de Física, Universidad Nacional del Sur (UNS), CONICET, AvAlem 1253, 8000 Bahía Blanca, Argentina

ABSTRACT

To predict electrical generation in piezoelectric small-scale beam energy harvesting devices, it is important to have a complete mathematical model that captures the different associated phenomena. In the literature, some authors propose several alternatives of non-linear mathematical formulations, with non-linearities coming from different physical aspects. All these formulations present good aptitudes to predict the nonlinear behavior of the system under different values of accelerations, geometry and boundary conditions. At the same time, they do not represent a unified general proposal for modeling multimodal energy harvesting devices of any type of mode generation and boundary conditions at large excitations. In this sense, this paper presents a mathematical description of inextensional nonlinear Euler-Bernoulli piezoelectric beams that combines the best contributions of the literature to the voltage generation of multimodal nonlinear piezoelectric energy harvesters (geometric, material and damping non-linearities). The developed analytical model yields a total set of $N + 1$ ordinary differential equations for the first N modes and for the output voltage. However, direct solution of this ordinary nonlinear differential system of N equations is computationally costly. Instead, a reduced algebraic system of $2(N + 1)$ algebraic equations is proposed applying the method of averaging. Its main advantage is that it makes more suitable and computationally economical for the implementation of a parameter identification process involving any number of piezoelectric inserts (unimorph or bimorph) and mode of generation (d_{33} or d_{31}). Two types of validations are presented for some selected physical systems to test the validity of the assumptions: a numerical one, by the direct integration of the equations of motion and an experimental one. A final comparison between the results demonstrates the importance of the having a unified nonlinear model to predict the generated voltage in multimodal energy harvesters.

Keywords: Piezoelectric Energy Harvesting; Material, Geometrical and Damping Non-linearities; Multimodal systems; Reduced algebraic equations.

* Corresponding author; e-mail: mfebbo@uns.edu.ar.

1. INTRODUCTION

Energy harvesting is one of the fundamental issues in the technological application of small-scale energy sources for the industry.

In particular, the harvest of energy based on the deformation of a piezoelectric material [1]caused by the vibration of the motors of the transport vehicles, is of interest in this work. Various types of devices have been reported in the literature for this purpose, from simple cantilever beams [2] to sophisticated multimodal devices [3, 4]. However, none of them seems to be definitive in the technological application of these types of devices.

Regarding the mathematical formulations used to model micro-power generation systems, many researchers have developed linear models of energy harvesting devices such as Beeby et al. [5] and Erturk et al. [6]. These models mostly use the theory of Bernoulli-Euler for the structural beam elements under base acceleration, considering a linear constitutive piezoelectric equation and Rayleigh proportional damping [7]. However, these formulations are accurate only for low excitation amplitudes [6]. As the amplitude of the base acceleration increases, linear models overestimate the electrical generation in a resonant condition, due to the intrinsic non-linearity of piezoelectric materials [8]. For this reason, nonlinear models are essential to describe the dynamic behavior of these systems and to predict energy generation in piezoelectric energy harvesters, as considered by different authors.

Several analytical approaches have been applied to study this problem. Between them, some authors present their models considering only geometric nonlinearities due to large displacements [9]. Other authors, instead, focus their studies modeling material nonlinearities such as the nonlinear elastic behavior, the nonlinear electromechanical coupling or ferroelastic and ferroelectric hysteresis [10-17]. Generally speaking, the addition or not of these nonlinear phenomena in the constitutive equations will depend on the strength of the electric field or the applied stress.

Concerning the proposals of non-linear constitutive equations, Joshi [10] presented in 1992 non-linear constitutive relations for piezoceramic materials, which would later be the basis of many works on applied piezoelectricity. He deduced the constitutive equations from a thermodynamic viewpoint based on Gibbs free energy. His nonlinear second order relations include non-linear elasticity terms, non-linear elasto and electric-striction terms and non-linear permittivity effects. Later in 2006, Bertotti and Mayergoyz by one side [11] and Damjanovicby the other side [12] presented in two textbooks a meticulous study on the hysteresis phenomenon in piezoelectric and ferroelectric materials. Following a similar approach, Goldschmidtboeing et al. [13] analyzed the influence of ferroelastic hysteresis on cantilever beams of PZT material, mechanically excited at the base. On the other hand, Stanton et al. [8] experimentally validated a mathematical model taking into account the non-linearity corresponding to high-order elastic effects and non-linear coupling associated with an energy harvesting circuit. Aurelle et al. [14] studied the contribution of deformations and electromechanical coupling in the non-linear response of a piezoelectric beam under weak electric fields in order to focus their study on nonlinearities separately. Following this line, Albareda et al. [15] considered a high-order formulation in the thermodynamic potential from which non-linear constitutive equations for the voltage and high-order electrical displacement in the deformation and electric field are obtained. Priya et al. [16] analyzed electrical non-linearities generated by strong electric fields and the influence of the ferroelastic phenomenon. Leadenham and Erturk [17] studied a model of

distributed parameters taking into account the softening effect and dissipative non-linearities caused by ferroelastic hysteresis of a bimorph piezoelectric beam of PZT 5A connected in series in its first flexional mode using the method of averaging. This formulation for the piezoelectric material was experimentally validated, both in actuation and in energy harvesting applications.

The need to unify these non-linear models in a single work that combines the best characteristics of previous contributions for a general multimodal system constitutes the aim of this paper. In this sense, this work proposes a generalized and unified non-linear mathematical model that combines the quadratic non-linear viscous dissipation proposed by Stanton et al. [8], the non-linear constitutive model proposed by Leadenham and Erturk [17] and a geometric non-linearity due to large deformations such as the one reported by Mak et al. [9]. In summary, the proposed model is capable to capture the physical phenomena that are observed in piezoelectric materials for energy harvesting due to large excitation amplitudes by the modification of its geometric, dissipative, structural and electrical characteristics. This includes the analytical description of d_{31} or d_{33} piezoelectric modes and unimorph or bimorph configurations in a beam-type structural element using an arbitrary number of structural modes for any type of boundary conditions. Additionally, the system of $N + 1$ differential equations obtained from the model is reduced to a 2 $(N + 1)$ generalized system of algebraic equations by means of the method of averaging. The numerical and experimental validation of the proposal is also presented for three different cases using a Macro Fiber Composite (MFC) piezoelectric sheet.

The paper is organized as follows. A detailed mathematical treatment of a multimodal device [18] consisting of a composite beam (piezoelectric + substructure) with two mass-spring systems attached to their ends which serves as a general application of the proposed formulation is presented in section 2.

Section 3 presents the reduction of the system of ordinary differential equations to a system of algebraic equations, using the method of averaging [19]. The obtained system is validated for electromechanical devices under any type of piezoelectric inserts and their physical configurations (unimorph or bimorph). Finally, section 4 presents the reduced system which is computationally and experimentally validated for a cantilever system in d_{31} and d_{33} mode generation as well as for the proposed multimodal system.

Concluding remarks summarize the main findings of the present proposal at the end of the paper.

2. THEORETICAL MODEL AND ELECTROMECHANICAL EQUATIONS

In this section we present a detailed non-linear formulation of a multimodal energy harvesting device (MEHD) previously presented by the authors in [20] using a linear theory. Despite of this fact, the final general equations can be applied for any mode of generation (d_{31} or d_{33}) and physical configuration (unimorph-bimorph).

Figure1 shows the MEHD comprising a composite beam with two spring-mass systems at the ends of it. The natural frequencies of the device can be chosen by a proper selection of system's parameters. The composite beam is represented by a substructure (steel or aluminum) and a sheet of piezoelectric material on the upper surface of the substructure (unimorph configuration). After analyzing different commercially available options, a PZT-5A macro fiber composite (MFC) with interdigitated electrodes (manufactured by Smart-Materials, Inc) is used in the present study, since it presents important advantages over those conventionally used [20, 21].

In Figure1, $w(x,t)$ is the relative vertical deflection of the beam, $g(t)$ is the temporary excitation of the base, L is the total length of the composite beam and $m_{1,2}$, $k_{1,2}$ and $k_{t1,2}$ are

the masses and the vertical and torsional stiffness of the springs at the ends $x = 0$ and $x = L$ respectively. In addition, a, b_p, h_p, b_s and h_s are the distance from the bottom piezoelectric side to the neutral fiber, the width and thickness of the piezoelectric sheet, and the width and thickness of the substructure, respectively.

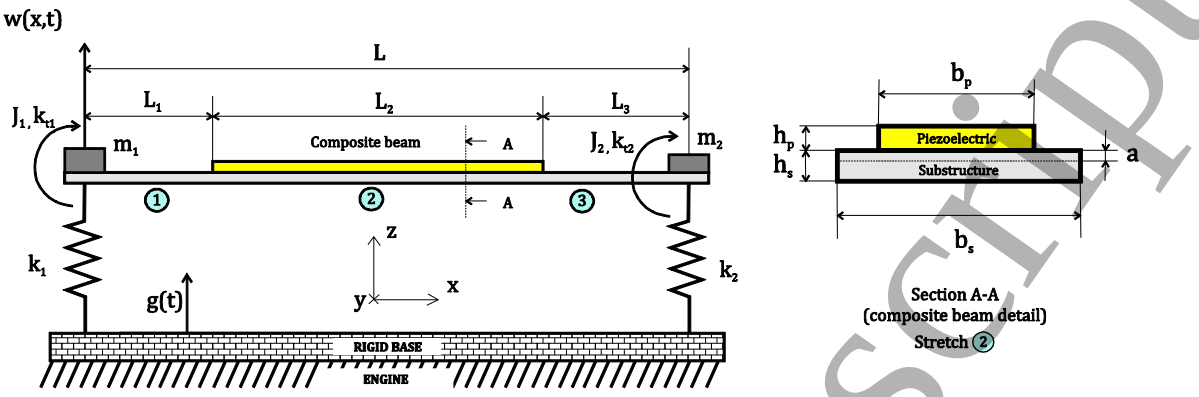

Figure1:Schematics of the model (left) with a detailed view of the composite beam (right).

On the other hand, Figure2 shows the basic electrical circuit that provides the voltage $v(t)$ generated by the device. There, it is possible to observe the electric model of the piezoelectric considered as a current generator $i(t)$, with an internal ideal capacitor C_p and a load resistance R_l connected in parallel.

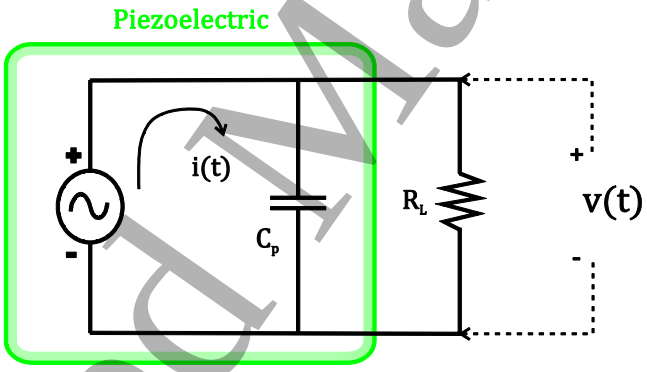

Figure2:Electrical equivalent circuit of a piezoelectric.

2.1. ELECTROMECHANICAL MODEL OF THE SYSTEM

The piezoelectric beam is modeled according to the Euler-Bernoulli formulation [22], considering only the vertical displacement and assuming that it is inextensible. This last assumption implies, for example, that it can not be applied for beams subject to large centrifugal forces, beams with fixed boundary conditions, etc [23].

A Lagrangian approach [24] is used to build up the system of differential equations. To consider the material nonlinearity, a similar model such as the one presented by Leadenham and Erturk [17] which considers a non-linear elasticity coefficient (c^p_{111}) and a non-linear coupling coefficient given by a non-linear piezoelectric constant (e_{333}) is used. However, in contrast to [17] a structurally more complex piezoelectric beam with interdigitated electrodes is used to carry out this study. Regarding the dissipation of energy in the MEHD, a viscous non-linear quadratic model is selected, as presented by Stanton et al. [8] for a structurally different type of piezoelectric material. This model demonstrates to have a good agreement with experimental tests in piezoelectric beam-like systems such as the one

presented in this work.

In the following, the axes x, y, z, shown in Figure1 correspond to the subscripts 1, 2 and 3, respectively. The points in the upper part of the variables ($\dot{}$, $\ddot{}$, ...) refer to the temporal derivatives, the quotes ($'$, $''$, ...) to the derivatives with respect to the coordinate x and the displacement in the z direction is $w(x,t)$. In addition, the superscripts p and s refer to the piezoelectric and substructure, respectively.

The displacement vector, without considering pure axial displacements and incorporating the temporal excitation of the base $g(t)$, is:

$$\boldsymbol{u} = [u_1 \quad u_2 \quad u_3]^t = [-zw' \quad 0 \quad w + g(t)]^t \tag{1}$$

The axial strain of a differential element is given by [24]

$$e = \sqrt{(1 + u'_1)^2 + u'^2_3} - 1 \tag{2}$$

After considering an inextensible beam $e = 0$, it is possible to obtain:

$$\begin{aligned} u'_1 &= -\frac{1}{2}u'^2_3 \\ u_1 &= -\frac{1}{2}\int_0^l u'^2_3 dl \end{aligned} \tag{3}$$

In this sense, non-linear geometric strains are given by the following local expression:

$$\varepsilon_1 = -z\left(w'' + \frac{1}{2}w''w'^2\right) \tag{4}$$

The first term on the right side of (4) is the axial strain of a problem of small displacements due to bending, while the second is the axial strain considering bending at large displacements.

The expression of the enthalpy density of the piezoelectric material (H^p) and of that the substructure (H^s) are defined as [17]:

$$\begin{aligned} H^p = \frac{1}{2}c^p_{11}{\varepsilon_1}^2 + \frac{1}{3}c^p_{111}{\varepsilon_1}^3 sign(\varepsilon_1) - e_{33}\varepsilon_1 E_1 - \frac{1}{2}e_{333}{\varepsilon_1}^2 E_1 sign(\varepsilon_1) \\ - \frac{1}{2}\epsilon^{\varepsilon}_{11}{E_1}^2 \end{aligned} \tag{5}$$

$$H^s = \frac{1}{2}c^s_{11}{\varepsilon_1}^2$$

Where $c^{p,s}_{11}$ are the elasticity modulus of the piezoelectric sheet and the substructure respectively, and $\epsilon^{\varepsilon}_{11}$ is the electric permittivity at constant strain. Additionally, $e_{33} = c^p_{11}d_{33}$ is the linear piezoelectric stress constant and E_1 is the longitudinal electric field in the x direction which is given by, $E_1 = -v(t)/\,l_p$ [20].

Applying the following relations [10]:

$$\sigma_1^p = \frac{\partial H^p}{\partial \varepsilon_1} \quad , \quad \sigma_1^s = \frac{\partial H^s}{\partial \varepsilon_1} \quad , \quad D_1 = -\frac{\partial H^p}{\partial E_1} \tag{6}$$

it is possible to obtain the axial stresses in the piezoelectric element ($\sigma_1^{p,s}$) and in the substructure which, as functions of the electric displacement (D_1) result:

$$\begin{gathered} \sigma_1^p = c_{11}^p \varepsilon_1 + c_{111}^p {\varepsilon_1}^2 sign(\varepsilon_1) - e_{33} E_1 - e_{333} \varepsilon_1 E_1 sign(\varepsilon_1) \\ \sigma_1^s = c_{11}^s \varepsilon_1 \\ D_1 = e_{33} \varepsilon_1 + \frac{1}{2} e_{333} {\varepsilon_1}^2 sign(\varepsilon_1) + \epsilon_{11}^{\varepsilon} E_1 \end{gathered} \tag{7}$$

Both expressions satisfy the necessary and sufficient condition [10]:

$$\frac{\partial \sigma_1^p}{\partial E_1} = -\frac{\partial D_1}{\partial \varepsilon_1} \tag{8}$$

It is important to clarify that the sign of the strain is incorporated in the quadratic terms in order to maintain the non-linear effect in both directions of the deformation of the beam.

The total potential energy of the system, neglecting the gravitational potential energy, is the sum of the elastic potential energies of the beam U_b and of the springs $U_{k1,2}$,

$U = U_b + U_{k1} + U_{k2}$.

The expression for the beam is given by [6]:

$$U_b = \int_{V_s} H^s dV_s + \int_{V_p} H^p dV_p \tag{9}$$

The first and second volume integral in (9) correspond to the elements of the substructure and the piezoelectric, respectively. Using expressions (4) and (5), replacing them in the equation (9) and integrating up to length L, we obtain:

$$\begin{aligned} U_b = \frac{1}{2} \int_0^L \Big[& EI {w''}^2 + \frac{1}{3} EI_n {w''}^3 sign(w'') + EI(w'w'')^2 \\ & - 2 \left(J_p(x) w'' + \frac{1}{2} J_{pn}(x) {w''}^2 sign(w'') \right. \\ & \left. + \frac{1}{2} J_p(x) {w'}^2 w'' \right) v(t) \Big] dx - \frac{1}{2} C_p v(t)^2 \end{aligned} \tag{10}$$

Where EI is the coefficient of linear stiffness which, for the sections 1 and 3 (see Figure1) is $EI_{1,3}$ and for section 2, which contains the piezoelectric sheet, it is EI_2. In addition, EI_n is the coefficient of non-linear stiffness valid only in section 2 due to the non-linear elasticity of the piezoelectric material. The expressions of these coefficients and those mentioned hereinafter are presented in Appendix A.

In view of equation (10) $J_p(x)$ is the coefficient of linear electromechanical coupling in section 2 due to the piezoelectric material, and it is defined as:

$$J_p(x) = J_p f_H(x) \tag{11}$$

where J_p is the linear electromechanical coupling constant and $f_H(x)$ is a function dependent on the generation mode (d_{31} o d_{33}) and the piezoelectric type (unimorph or bimorph). This function is introduced to consider the coupling only in the length of the piezoelectric sheet and to retain the corresponding term after the spatial differentiation. For a d_{33} generation mode, the electric field is assumed to be uniform in the longitudinal direction x over the effective electrode spacing, as considered in ref [31]. This leads to a linear function for the electric potential (voltage) over the length of the harvester, as can be seen in Figure 12 in the Appendix. Then, the function $f_H(x)$ results:

$$f_H(x) = \sum_{i=1}^{n} \left\{ \left(1 + \frac{x - x_{i2}}{x_{i2} - x_{i3}}\right)[H(x - x_{i2}) - H(x - x_{i3})] + \left(\frac{x - x_{i4}}{x_{i5} - x_{i4}}\right)[H(x - x_{i4}) - H(x - x_{i5})] \right\} \tag{12}$$

Where $H(x)$ is the Heaviside function and the x_{ij} can be seen in Figure12 of Appendix A.
For a d_{31} generation mode, the electric field is also assumed to be uniform in the vertical direction y, between the electrodes. In this sense, the voltage is constant at the top and bottom electrodes, as can be observed in Figure 14, in the Appendix. Then, the function $f_H(x)$ takes the form:

$$f_H(x) = \sum_{i=1}^{n} [H(x - x_{i1}) - H(x - x_{i1}) + H(x - x_{i3}) - H(x - x_{i4}) + H(x - x_{i5}) - H(x - x_{i6})]$$

Where $H(x)$ is the Heaviside function and the x_{ij} can be seen in Figure 14 of Appendix A.

In equation (10) $J_{pn}(x)$ is the coefficient of non-linear electromechanical coupling in section 2, and it is defined as:

$$J_{pn}(x) = J_{pn} f_H(x) \tag{13}$$

where J_{pn} is the non-linear coupling constant whose approximate expression, considering a constant electric field throughout the length of the piezoelectric, is presented in Appendix A.

To conclude with the potential energy of the beam, it should be clarified that for the nonlinear geometric terms, only the quadratic terms coming from ${\varepsilon_1}^2$ were taken into account. In addition, in order to obtain an approximate analytical expression for the sign function, only the component of small displacements of the deformation ($\varepsilon_1 = -zw''$) which represent its linear part, is considered for the sign function.

On the other hand, the elastic potential energy of the springs, taking into account the vertical and torsional deformation with respect to the y axis, turns out to be:

$$U_{ki} = \frac{1}{2}\left[k_i w(x_j, t)^2 + k_{ti} w'(x_j, t)^2\right] \quad , \quad i = 1,2 \quad , \quad x_j = 0, L \tag{14}$$

Similarly, the total kinetic energy of the system is the sum of the kinetic energies of the beam T_b and the tip masses at the ends of the beams $T_{m1,2}$.

Then, $T = T_b + T_{m1} + T_{m2}$. It should be noted that the rotational inertia of the beam is neglected. However, the rotational inertia of the tip masses is taken into account. Finally, the expression for the beam results [6]:

$$T_b = \frac{1}{2}\left(\int_{V_s} \rho_s(\dot{w} + \dot{g})^2 dV_s + \int_{V_p} \rho_p(\dot{w} + \dot{g})^2 dV_p\right) \quad (15)$$

where $\rho_{p,s}$ is the density of the piezoelectric and the substructure, respectively. Expanding equation (15) and integrating for a length L, we obtain:

$$T_b = \frac{1}{2}\int_0^L (\rho A\dot{w}^2 + 2\rho A\dot{w}\dot{g})dx + \frac{1}{2}m_t\dot{g}^2 \quad (16)$$

Where ρA is the unitary mass of the beam, given by: $\rho A_{1,3}$ for sections 1 and 3, and $\rho A_2$for section 2. In the last term of equation (16), m_t is the total mass of the beam.
The kinetic energy of the masses, taking into account the vertical displacement and their rotational inertias results:

$$T_{mi} = \frac{1}{2}\left\{m_i\left[\dot{w}(x_j,t) + \dot{g}\right]^2 + J_i\dot{w}'(x_j,t)^2\right\} \quad , \quad i = 1,2 \quad , \quad x_j = 0, L \quad (17)$$

As already mentioned above, for the dissipation of energy in the device, two types of effects are considered: (a) viscous damping in the composite beam and (b) dissipation by Joule effect [25] in the load resistance. For the viscous damping, a linear and a nonlinear quadratic model is proposed, following Stanton [8], Bandstra [26] and Yang [27] adopting the form:

$$F_v = c\dot{w} + c_n\dot{w}^2 sign(\dot{w}) \quad (18)$$

where c and c_n are the linear and non-linear damping coefficients respectively.

In order to apply Hamilton's principle for deducing the electromechanical equations, we include these dissipation effects via the work of non-conservative forces δW_{nc} resulting in:

$$\delta W_{nc} = -F_v\,\delta w - i\,\delta\lambda \quad (19)$$

Where λ is the electric flow and the electric current i is calculated by Ohm's Law as $i = \dot{\lambda}/R_l$ where $\dot{\lambda} = v$ is the voltage in the load resistance.

2.2. **Electromechanical Lagrange Equations**

Applying Hamilton's principle we obtain the Lagrange equations [24] for the system considered:

$$\frac{\partial}{\partial t}\left(\frac{\partial L}{\partial \dot{w}}\right)+\frac{\partial}{\partial x}\left(\frac{\partial L}{\partial w'}\right)-\frac{\partial}{\partial x^2}\left(\frac{\partial L}{\partial w''}\right)+c\dot{w}+c_n\dot{w}^2 sign(\dot{w})=0 \tag{20}$$

$$\frac{\partial}{\partial t}\left(\frac{\partial L}{\partial v}\right)+\frac{v}{R_l}=0 \tag{21}$$

where the Lagrangian is $L=T-U$.

Then equation (20) becomes:

$$\begin{aligned}\rho A\ddot{w}+c\dot{w}+c_n\dot{w}^2 sign(\dot{w})+EIw^{IV}+EI_n(w'''^2+w''w^{IV})sign(w'')\\ +EI(w''^3+4w'w''w'''+w'^2w^{IV})-J_p''v\\ -vJ_{pn}w^{IV}sign(w'')-v\left(J_p'w'w''+\frac{1}{2}J_p''w'^2\right)=-\rho A\ddot{g}\end{aligned} \tag{22}$$

and equation (21) turns into:

$$\begin{aligned}C_p v+\frac{v}{R_l}+\int_0^l\left[\left(J_p+J_{pn}w''sign(w'')+\frac{1}{2}J_p w'^2\right)\dot{w}''+J_p w'w''\dot{w}'\right]dx\\ =0\end{aligned} \tag{23}$$

These expressions are a generalization of others previously proposed in the literature, particularly for the nonlinear terms. The equation proposed by Leadenham and Erturk [17] can be recovered by neglecting the nonlinear geometrical terms (sixth term of the left hand side in Eq. 22 and fifth and sixth terms of the left hand side in Eq. 23) and modifying the damping terms (second and third terms of the left hand side in Eq. 22) by his own proposal. Additionally, there is a difference in the last term of the left hand side in Eq. 22 due to $f_H(x)$, which depends on the interdigitated electrodes of the MFC (Leadenham and Erturk [17] used a piezo sheet T226-A4-103X with no fibers). On the other hand, the equations proposed by Stanton et al. [8] can be obtained by eliminating the sign function and the nonlinear geometrical terms in Eqs. 22 and 23.

2.3. **Spatial discretization of electromechanical equations**

One of the main procedures to obtain an analytical solution of the Lagrange equations for continuous media is the spatial discretization of the displacement, applying the classical method of modal expansion by separation of variables. In this method, the deflection of the beam is represented as a finite sum of N generalized coordinates $q_i(t)$ multiplied by modal shape functions $\phi_i(x)$as follows:

$$w(x,t)=\sum_{i=1}^{N}\phi_i(x)\,q_i(t) \tag{24}$$

Modal shape beam-type functions are proposed of the following form:

$$\phi_i(x)=C_1\cos(\beta_i x)+C_2\cosh(\beta_i x)+C_3\sin(\beta_i x)+C_4\sinh(\beta_i x) \tag{25}$$

where the eigenvalues β_i are related to their respective natural frequencies ω_i by $\omega_i=(\beta_i L)^2\sqrt{EI/\rho AL^4}$ and the constants $C_j(j=1-4)$ are determined by the boundary

conditions and normal mode normalization condition [18].

Replacing equation (24) in (22), multiplying both members by $\phi_i(x)$ and integrating in the total length L, we obtain a set of $i = 1..N$ equations of the form:

$$\begin{aligned} M_i\ddot{q}_i + C_i\dot{q}_i + \sum_{j,k=1}^{N} C_{nijk}\dot{q}_j\dot{q}_k sign(\dot{q}_j) + K_i q_i + \sum_{j,k=1}^{N} K_{nijk} q_j q_k sign(q_j) \\ + \sum_{j,k,l=1}^{N} K_{Gijkl} q_j q_k q_l \\ - \left(\theta_i + \sum_{j=1}^{N} \theta_{nij} q_j sign(q_j) + \sum_{j,k=1}^{N} \theta_{Gijk} q_j q_k\right) v \\ = -M_{ai}\ddot{g} \end{aligned} \tag{26}$$

Similarly, using (24) in (23), an electromechanical equation for the voltage v can be obtained:

$$C_p\dot{v} + \frac{v}{R_l} + \sum_{i=1}^{N}\left(\psi_i + \sum_{j=1}^{N} \psi_{nij} q_j\, sign(q_j) + \sum_{j,k=1}^{N} \psi_{Gijk} q_j q_k\right)\dot{q}_i = 0 \tag{27}$$

Equation (26) and (27) are the governing electromechanical equations of the energy harvesting model. It is important to note that the terms involving the electromechanical couplings ψ and θ are different because in this case the electrodes of the piezoelectric sheet do not cover the entire length of the substructure. This situation differs from most works in the literature where the electrode covers the entire surface of the piezoelectric or where this approach is considered valid as an approximation to the real problem.

3. REDUCTION OF EQUATIONS

The system of differential equations (26)-(27) is constituted by $N + 1$ differential equations, where N is the number of modes. The direct integration of these equations via a numerical method demands an increasingly large time as the number of modes increases, making the problem hard to solve. To overcome this drawback, in this section we propose to reduce the entire non-linear model to a system of algebraic equations by applying the averaging method [19]. The resulting system consists of two subsystems of N mechanical equations, plus two coupled electrical equations, constituting a system of $2(N + 1)$ algebraic equations which is computationally economical to solve. An additional advantage lies in the fact that it is easier and faster to apply methods of identification of parameters and optimization methods to improve power generation. However, the reduction is valid for problems in absence of internal resonances between modes. Despite of this drawback, the multimodal character of the reduced solution permits to consider the contribution of N modes to problem, unlike a large body of research work conducted to date [13,14,17].

The averaging method has been widely used to analyze periodic solutions of ordinary non-linear differential equations. A solution is assumed in sines and cosines, replacing the ordinary differential equations by algebraic equations. Then, the error in the approximate solution is minimized with the Galerkin method [29]. Finally, the resulting system of algebraic equations is solved iteratively, with methods such as Newton-Raphson.

To perform the reduction of equations (26)-(27) applying this method, we first propose a harmonic base acceleration of the form $\ddot{g}(t) = G\,cos(\Omega t)$ and then assume that the temporal response of the mode $i, q_i^*(t)$ and of the voltage $v(t)$, is harmonic of the form:

$$q_i^*(t) = q_i\,cos(\Omega t + \phi_i)$$
$$v(t) = V\,cos(\Omega t + \phi) \tag{28}$$

These equations can be expressed in an equivalent way by means of the following trigonometric relations:

$$q_i\,cos(\Omega t + \phi_i) = Q_{(2i-1)}\,cos(\Omega t) + Q_{(2i)}\,sin(\Omega t)$$
$$V\,cos(\Omega t + \phi) = V_1\,cos(\Omega t) + V_2\,sin(\Omega t) \tag{29}$$

where

$$cos(\phi_i) = \frac{Q_{(2i-1)}}{q_i}\ ,\ \ sin(\phi_i) = \frac{Q_{(2i)}}{q_i}\ ,\ \ cos(\phi) = \frac{V_1}{V}\ ,\ \ sin(\phi) = \frac{V_2}{V} \tag{30}$$

from which the displacement modal amplitudes q_i and voltage V can be defined as:

$$q_i = \sqrt{Q_{(2i-1)}^2 + Q_{(2i)}^2}$$
$$V = \sqrt{V_1^2 + V_2^2} \tag{31}$$

Substituting equations (28) and the expression for $\ddot{g}(t)$ into equations (26)-(27) and applying the averaging method yields the following set of $2(N+1)$ algebraic equations in $Q_{(2i-1)}, Q_{(2i)}, V_1, V_2$:

$$\begin{aligned} -M_i\Omega^2 Q_{(2i-1)} + C_i\Omega Q_{(2i)} + K_i Q_{(2i-1)} - \theta_i V_1 + \frac{8}{3\pi}C_n^*\Omega^2 Q_{(2i)} \\ + \frac{8}{3\pi}K_n^* Q_{(2i-1)} \\ + \frac{4}{3\pi}\theta_n^*\left[\left(2Q_{(2i-1)}^2 + Q_{(2i)}^2\right)V_1 + Q_{(2i-1)}Q_{(2i)}V_2\right] \\ + \frac{3}{4}K_G^* Q_{(2i-1)} \\ + \frac{1}{4}\theta_G^*\left[V_1\left(3Q_{(2i-1)}^2 + Q_{(2i)}^2\right) + 2Q_{(2i-1)}Q_{(2i)}V_2\right] + F_i \\ = 0 \end{aligned} \tag{32}$$

$$-M_i\Omega^2 Q_{(2i)} - C_i\Omega Q_{(2i-1)} + K_i Q_{(2i)} - \theta_i V_2 - \frac{8}{3\pi}C_n^*\Omega^2 Q_{(2i-1)} + \frac{8}{3\pi}K_n^* Q_{(2i)} + \frac{4}{3\pi}\theta_n^*\left[\left(Q_{(2i-1)}^2 + 2Q_{(2i)}^2\right)V_2 + Q_{(2i-1)}Q_{(2i)}V_1\right] + \frac{3}{4}K_G^* Q_{(2i)} + \frac{1}{4}\theta_G^*\left[V_2\left(Q_{(2i-1)}^2 + 3Q_{(2i)}^2\right) + 2Q_{(2i-1)}Q_{(2i)}V_1\right] = 0 \quad (33)$$

$$C_p\Omega V_2 + \frac{V_1}{R_l} + \Omega\sum_{i=1}^{N} Q_{(2i)}\left[\psi_i + \frac{4}{3\pi}\psi_n^* + \frac{1}{4}\psi_G^*\right] = 0 \quad (34)$$

$$C_p\Omega V_1 - \frac{V_2}{R_l} + \Omega\sum_{i=1}^{N} Q_{(2i-1)}\left[\psi_i + \frac{4}{3\pi}\psi_n^* + \frac{1}{4}\psi_G^*\right] = 0 \quad (35)$$

which constitute the reduced system of differential equations that model the behavior of flexural Euler-Bernoulli beams with electromechanical (piezoelectric) inserts in any type of generation mode (d31 o d33) and piezoelectric configuration (unimorph or bimorph). In the previous equations, the following coefficients are defined:

$$C_n^* = \frac{q_1}{q_i}\sum_{j,k=1}^{N} A_{jk}C_{nijk} \quad , \quad K_n^* = \frac{q_1}{q_i}\sum_{j,k=1}^{N} A_{jk}K_{nijk} \quad , \quad K_G^* = \frac{q_1}{q_i}\sum_{j,k,l=1}^{N} q_j A_{kl}K_{Gijkl}$$

$$\theta_n^* = \frac{q_1}{q_i^3}\sum_{j=1}^{N} A_{ij}\theta_{nij} \quad , \quad \theta_G^* = \frac{q_1}{q_i^2}\sum_{j,k=1}^{N} A_{jk}\theta_{Gijk} \quad , \quad \psi_n^* = \sum_{j=1}^{N} q_j\psi_{nij} \quad , \quad \psi_G^* = q_1\sum_{j,k=1}^{N} A_{jk}\psi_{Gijk}$$

where $A_{ij} = A_{jk} = A_{kl}$ are the components of the so-defined amplitude coefficient matrix $\boldsymbol{A}$, which is expressed as:

$$\boldsymbol{A} = \begin{bmatrix} \frac{q_1^2}{q_1} & \frac{q_1 q_2}{q_1} & \cdots & \cdots & \frac{q_1 q_N}{q_1} \\ & \ddots & & & \frac{q_2 q_N}{q_1} \\ & & \ddots & & \vdots \\ & & & \ddots & \vdots \\ Sym & & & & \frac{q_N^2}{q_1} \end{bmatrix} \quad (36)$$

4. NUMERICAL AND EXPERIMENTAL VALIDATION

In order to validate the results presented in section (3), here we compare the solutions obtained by the reduced system, equations (32)-(35), to those obtained by direct integration of the equations of motion (Eqs. 22-23) and to experimental results. This is

carried out for the following cases: a cantilever beam in d_{33} and d_{31} generation mode and the multimodal device presented in section 2. For the numerical validation, the reduced system is solved iteratively using the method of least squares by means of the trust-interval algorithm (trust-region) implemented by Matlab® *fsolve* command. On the other hand, the system of differential equations is integrated numerically through the implementation of an explicit Runge-Kutta formula by the variable step algorithm of Dormand-Prince [30], through the command *ode45* of Matlab®. For the experimental measurements, the systems are excited by its base through an electrodynamical shaker with variable frequency, waveforms and acceleration levels, and the voltage and accelerations are acquired via PCB accelerometers (model 80C) and a NI data acquisition system (model 9230) at a rate of 2048 samples/sec.

4.1. CANTILEVER d_{33} BEAM

The cantilever beam of Figure 3 is selected for the first case experimental and numerical validation of the reduced equations. A piezoelectric sheet MFC 8507-P1 bonded over a steel beam constitutes the piezoelectric system which generates in d_{33} mode.

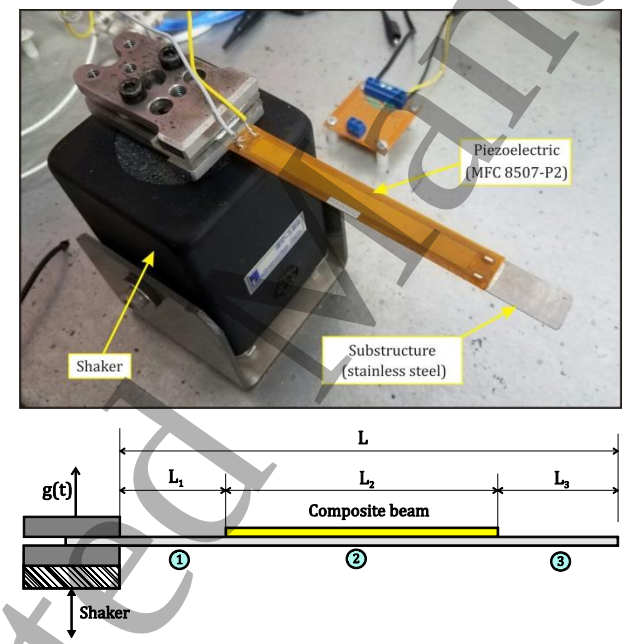

Figure 3: Schematic representation of the cantilever model and experimental setup.

Numerical values of the physical parameters of the cantilever system can be found in Table 1.

To obtain the linear and nonlinear coefficients that were introduced in the analytical model, we carry out an identification process. This process was performed in two stages, minimizing the norm of the difference between theoretical and experimental data over a region that includes the first mode of a cantilever d_{33} beam. The first stage includes the identification of the linear coefficients at very low (constant) acceleration amplitude of 0.04 g (g=9.8 m/s²) with an electrical load of 255 kΩ. As a result, the linear coefficient ξ_1 and the correction factors α (included in the definition of matrices θ, θ_n, θ_G) and β (included in ψ, ψ_n y ψ_G) were simultaneously identified.

The second stage devotes to identify the nonlinear coefficients. To this end, the numerical values of linear coefficients identified in the first stage were introduced into the model. Then, we performed the identification process at 1 g of constant acceleration amplitude with an electrical load of 255 kΩ. As a result, the nonlinear coefficients ξ_{n1}, c^{p}_{111} and e_{333} were simultaneously identified.

Several tests were performed at constant base acceleration with values of 1, 0.5, 0.1 and 0.04 G, while measuring the stationary voltage in the range of 14-26 Hz. Figure 4 shows the results for: the experimental cases (circles), the reduced model considering only one mode of vibration (Eqs. 32-34 for N = 1, solid lines) and the curves obtained by direct integration of the equations of motion (Eqs. 26-27) for N=1 and N=3, which are plotted as dashed lines and dash-dotted lines, respectively.

Coefficient	Value	Coefficient	Value
L_1	17.6 mm	ρ_s	7900 kg/m^3
L_2	85 mm	ρ_p	7750 kg/m^3
L_3	21.8 mm	c^s_{11}	193 GPa
L	124.4 mm	c^p_{11}	61 GPa
a	0.176 mm	c^p_{111}	0
h_s	0.38 mm	d_{33}	440 pm/V
b_s	12.7 mm	e_{333}	6.5663×10^4
h_f	0.18 mm	$\epsilon^{\varepsilon}_{11}$	15.3 nF/m
b_f	0.355 mm	C_p	1.5 nF
h_k	0.06 mm	ξ_1	0.0115
l_p	0.41 mm	ξ_{n1}	1.387×10^{-4}
w_p	0.097 mm	α	0.2
n_f	18	β	0.2

Table 1: Material and geometric parameters of the cantilever model (d_{33} generation).

From the results it can be observed that both, the reduced system and the direct integration of the ODES present a good agreement between them and, in turn, fit satisfactorily to the experimental values. This implies that the reduced system predicts with good accuracy the output voltage for different acceleration amplitudes, including those cases not considered in the identification process. Regarding the number of modes assumed in the solution, the direct integration of the ODES shows no sensitive difference to this number. It is important to note that, for the maximum value of acceleration (1G), a hardening nonlinearity is evidenced for this type of physical system.

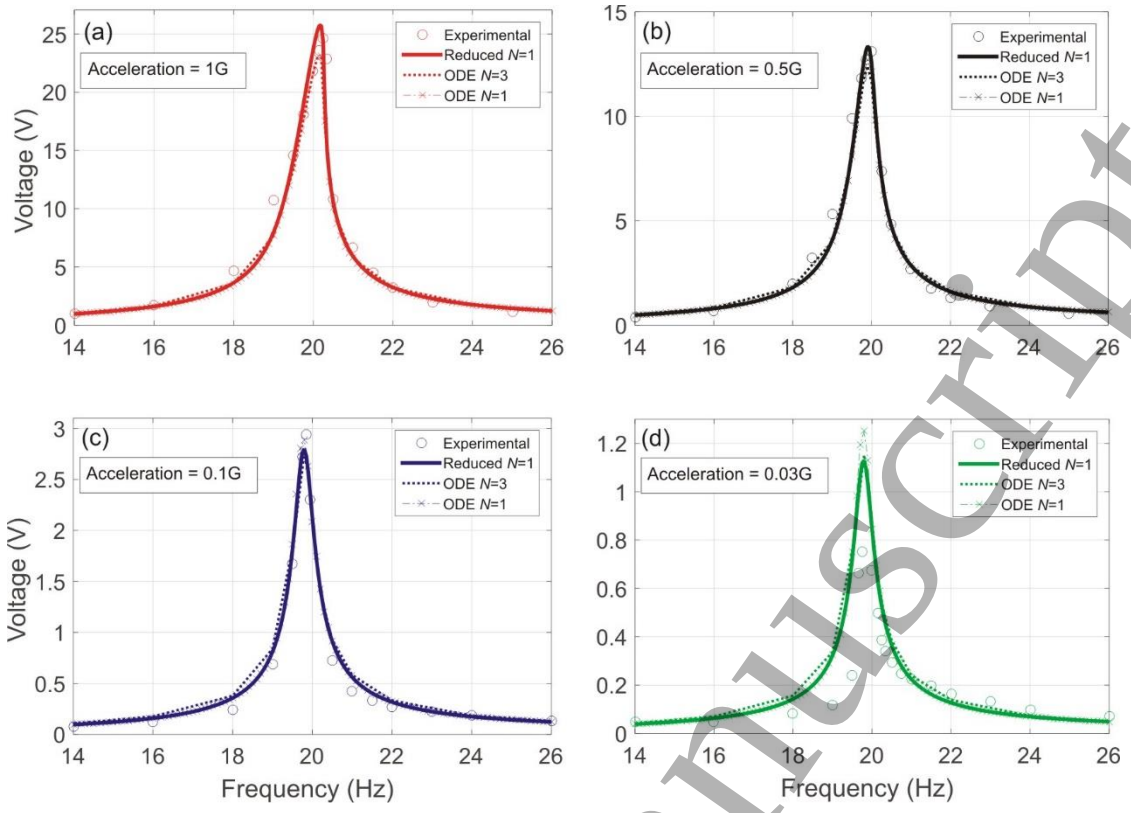

Figure 4: Output voltage for different methods: reduced model with N=1 (Reduced N=1), direct integration of the equations of motion with N=1 and N=3 (ODE N=1 and ODEN=3), and experimental results for a cantilever beam in d_{31} generation mode.(a) for 1g of base acceleration, (b) for 0.5g of base acceleration, (c) for 0.1g, and (d) for 0.03g (g=9.8 m/s^2).

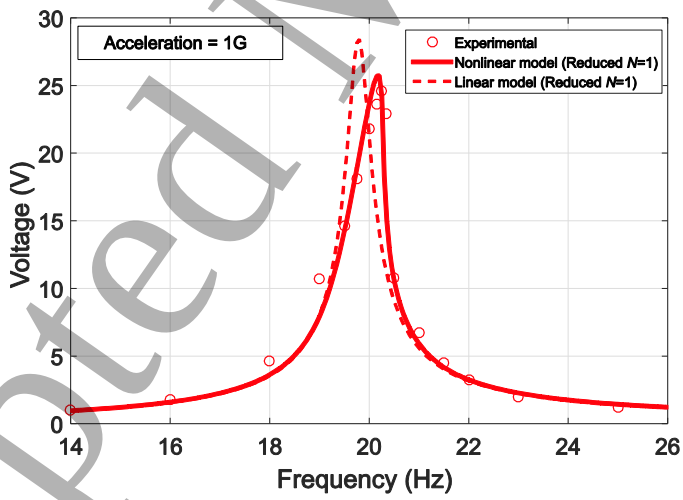

Figure 5: Comparison between linear and nonlinear model in d_{33} generation mode.

Figure 5 presents the comparison with a linear model which is implemented equating to zero the nonlinear terms of the reduced equations (32)-(35)with $N = 1$. From the results, it is possible to observe an overestimation of the generated voltage by an amount of more than 3 Volts, which represents more than 10% of the predicted value of the nonlinear model.

4.2. CANTILEVER d_{31} BEAM

In a similar manner, a cantilever beam with a piezoelectric sheet MFC 8507-P2 is used to

build the piezoelectric system which generates in d_{31} mode.

Table 2 shows the numerical values of the physical parameters of the cantilever system.

Following the same approach presented in section 4.1, the linear and nonlinear coefficients were obtained from an identification process following two stages. In the first stage, the linear parameters ξ_1 and γ were identified at very low (constant) acceleration amplitude of 0.04 g and electrical load of 255 kΩ. The second stage identified the nonlinear coefficients ξ_{n1}, c_{111}^{p} and e_{311} . The identification process was carried out at 1 g of constant acceleration amplitude using the linear parameters obtained in the first stage and the same electrical load of 255 kΩ.

Coefficient	Value	Coefficient	Value
L_1	17.2 mm	c_{11}^{s}	193 GPa
L_2	85 mm	c_{11}^{p}	61 GPa
L_3	21.5 mm	c_{111}^{p}	-2.685×10^{12}
L	123.7 mm	d_{31}	$-190\ pm/V$
a	0.176 mm	e_{311}	9.4553×10^{3}
h_s	0.38 mm	$\epsilon_{33}^{\varepsilon}$	16.81 nF/m
h_p	0.3 mm	C_p	49 nF
b_s	12.7 mm	ξ_1	0.0059
b_p	8 mm	ξ_{n1}	3.0071×10^{-4}
ρ_s	7900 kg/m^3	γ	0.65
ρ_p	7750 kg/m^3		

Table 2: Material and geometric parameters of the cantilever model (d_{31} generation).

Figure 5 shows the results at constant base acceleration considering 1, 0.5, 0.1 and 0.04 G, while measuring the stationary voltage in the range 14-26 Hz. A very good agreement is observed for all the analyzed cases. This is, the experimental curves (circles), the reduced model curves with one mode (N = 1, solid lines) and the curves which are the result of the direct integration of the equations of motion with 1 and 3 modes (N = 1, dashed lines, N = 3, dash-dotted lines). In contrast with the d_{33} case, a softening nonlinearity can be observed for the maximum considered acceleration of 1G. Additionally, the generated voltage is larger in comparison with the previous case (d_{33}). For example, for a base acceleration of 1G, the maximum voltage is 46 V for the MFC 8507-P2 (d_{31}) and 26 V for the MFC 8507-P1 (d_{33}). This difference is still larger for lower accelerations, for example 0.1 G, getting values of 9 and 3 V for MFC 8507- P2 and MFC 8507- P1, respectively.

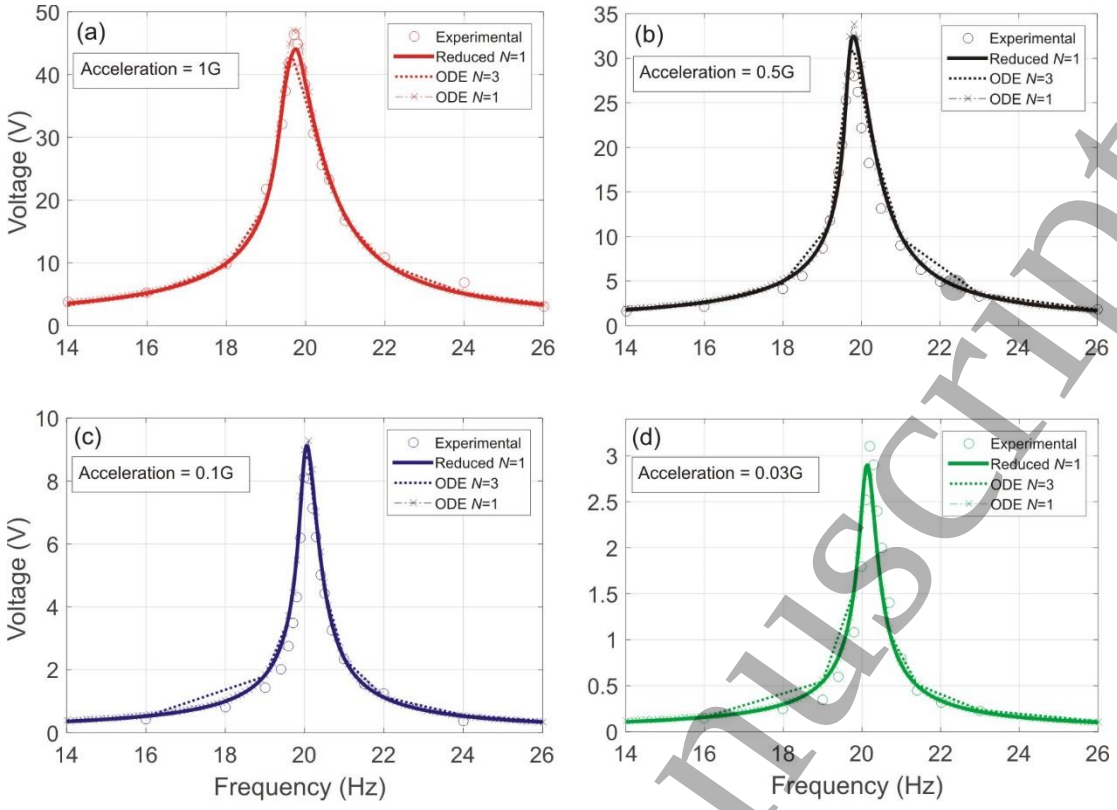

Figure 6: Output voltage for different methods: reduced model with N=1 (Reduced N=1), direct integration of the equations of motion with N=1 and N=3 (ODE N=1, ODE N=3), and experimental results for a cantilever beam in d_{31} generation mode. (a) for 1g of base acceleration, (b) for 0.5g of base acceleration, (c) for 0.1g, and (d) for 0.03g (g=9.8 m/s^2)

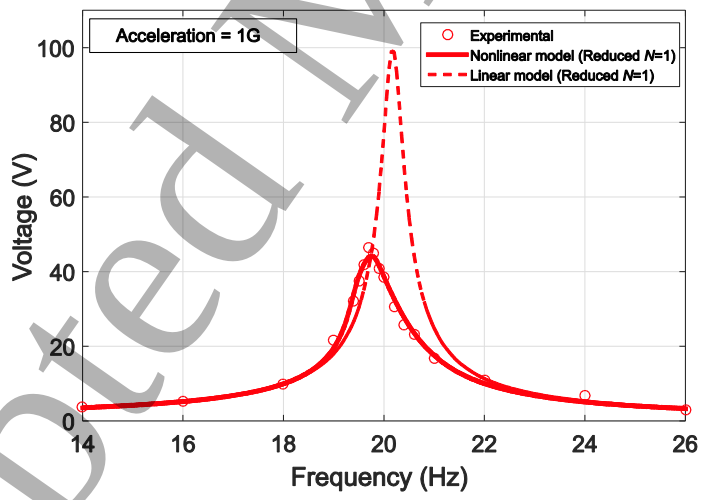

Figure 7: Comparison between linear and nonlinear model in d_{31} generation mode.

Similarly, Figure 7 presents the comparison with a linear model. This time, the overestimation of the generated voltage is notably larger compared with the d_{33} case. It is possible to observe a difference of more than a 100% between the nonlinear predictions, the experiments and the linear values for an acceleration of 1 G.

Figure 8 presents the contribution to the voltage of the nonlinear terms of equations (26)-(27) in d_{31} generation mode. The different terms are labelled according to the coefficients presented in table 2: ξ_{n1} (quadratic damping coefficient) represents the nonlinear damping

term (third term in the LHS of equation 26), c_{111}^{p} (nonlinear elasticity coefficient) characterizes the nonlinear restoring force (fifth term in the LHS of equation26), e_{311} (nonlinear piezoelectric constant) represents the nonlinear electromechanical coupling (eighth term in the LHS of equation 26) and *nonlin-geom* characterizes the nonlinear geometric terms (sixth and ninth terms in the LHS of equation 26).

To better discuss the results, some contributions are presented individually and others are added to each other in Figure 8. For example, the contribution of the nonlinear damping term ξ_{n1}, (blue dashed line) is presented alone. Instead, the contribution labelled by ξ_{n1} $+c_{111}^{p}$(red dashed line) represents the combined effect of the nonlinear damping term and the nonlinear restoring force. It is interesting to observe the influence of each term to the voltage response $V(\omega)$. Regarding the nonlinear damping term, it can be clearly observed that it is not capable by itself to dampen sufficiently the response to fit the experimental data. Additionally, the nonlinear geometric terms bend the response peak to the right (typical of a hardening behavior) while the nonlinear restoring force gives a totally different (softening) response. However, compared to the experimental data, a fundamental contribution of the nonlinear electromechanical coupling appears to be necessary to match the measurements. In this sense, there is an additional damping provided by this term as can be clearly observed from Figure 8 ($\xi_{n1} + e_{311}$ green squares).

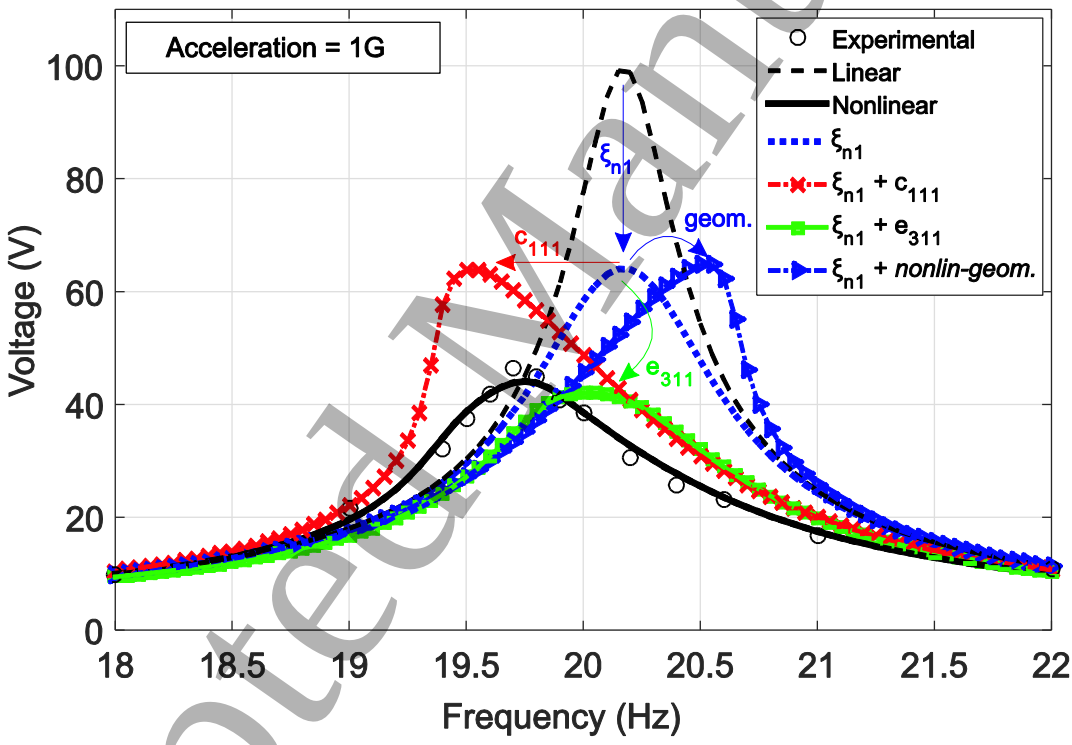

Figure 8: Contribution to the voltage of the nonlinear terms of Eqs. 26-27 in d_{31} generation mode.

4.3. MULTIMODAL DEVICE

The last configuration tested in this section is the multimodal device developed in section 2with a piezoelectric sheet MFC 8507-P1 (see Figure1). In this case, only numerical predictions will be compared. The interesting point inthis case is the possibility to validate

the reduced nonlinear model for a multimodal device. To this end, the reduced model (Eqs. 32-34) with N=3 (red solid lines), the linear model (red dashed lines) and the direct integration of the equations of motion (Eqs. 26 and 27) with N=3 (blue dotted lines) are shown in Figure 6. The numerical values of the geometrical, mechanical and material parameters used in both methods are presented in Table 3.

From the analysis of the results, it is possible to conclude that the linear model always overestimates the voltage generation, especially for the first and third modes.

Considering the nonlinear model, a good general agreement between the curves is observed for the three modes. However, there are some frequency regions wherethe reduced model overestimates the voltage obtained from the direct integration values, particularly for the second and third mode.

Coefficient	Value	Coefficient	Value	Coefficient	Value
L_1	23.3 mm	a	0.176 mm	ξ_{n1}	1.387×10^{-4}
L_2	85 mm	ρ_s	7900 kg/m^3	ξ_1	0.011
L_3	17.2 mm	ρ_p	5440 kg/m^3	ξ_2	0.039
L	125.5 mm	c_{11}^s	193 GPa	ξ_3	0.008
h_s	0.38 mm	c_{11}^p	15.85 GPa	m_1	19.1 g
b_s	12.7 mm	C_p	2.37 nF	m_2	6.09 g
h_f	0.18 mm	d_{33}	440 pm/V	k_1	4708 N/m
b_f	0.355 mm	$\epsilon_{11}^{\varepsilon}$	7.01 nF/m	k_2	3217 N/m
h_k	0.06 mm	α	0.2	k_{t1}	0.54 Nm/rad
l_p	0.41 mm	β	0.2	k_{t2}	0.36 Nm/rad
w_p	0.097 mm	c_{111}^p	0	J_1	3.35×10^{-7} kg/m^2
n_f	18	e_{333}	6.5663×10^4	J_2	5.86×10^{-8} kg/m^2

Table 3: Material and geometrical parameters of the model.

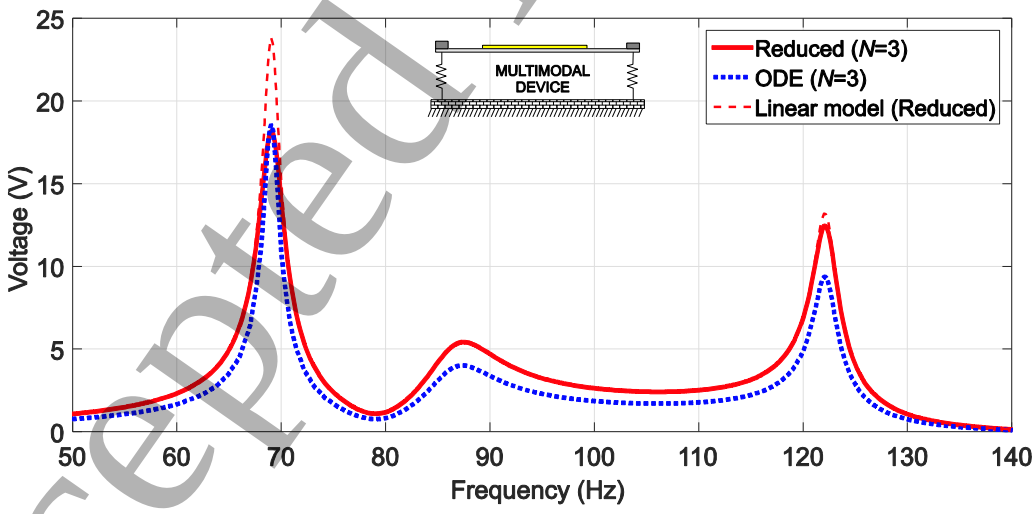

Figure9: Comparison of voltage curves for N=3 between the reduced model and the direct integration of the equations of motion (ODE).

Then, it is worth to analyze the sources of these deviations. If we look at section 3, equation (28), it is possible to observe that only the first harmonic is taking into account in the reduced model. To analyze the consequences of this approach, Figure10shows the steady state of the output voltage and its spectrum (coming from the direct integration of

the equations of motion) in a temporal interval of 0.1 seconds for two different excitation frequencies: 100 and 122 Hz. From the figure, it is possible to observe that the steady state response seems to have a sinusoidal appearance for both analyzed cases. This is confirmed by its spectrum which is shown in the bottom part of the same figure. In this case, the contribution of the first harmonic represents almost the 90% of the total amplitude for both excitation frequencies. As a consequence, it is almost irrelevant for the present case to take higher harmonics in the approximate solution for the reduction of the system. Another source of possible discrepancy between the methods is the approximation of the sign function assumed in the approximate analytical solution provided by the reduction of the equations.

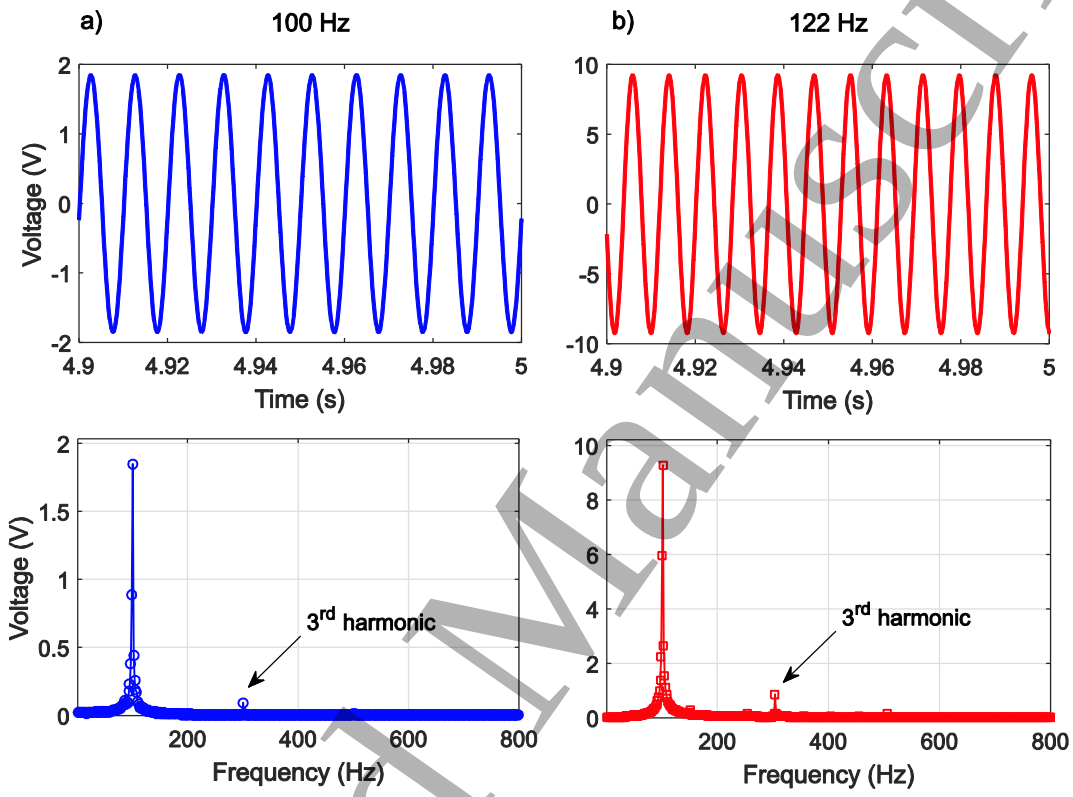

Figure10: Temporal response and spectrum at a)100 Hz (off-resonance)andb) 122 Hz (resonance).

In order to show the importance of the reduced model, Table4 shows the computational calculation times to solve each system as a function of the number of modes. In addition, it shows the relative percentage that it takes to solve the ODES. From the times observed in the first and second columns, it can be clearly deduced that the time it takes to solve a system with $N = 3$ represent 5.5% of the time tosolve the ODE. And this difference is increased when increasing the number of modes, reaching 1.7% when $N = 6$.

	Time (seconds)		Reduced relative to ODE
	ODE	Reduced	
$N = 3$	271.11	15.02	5.54 %
$N = 4$	515.69	20.69	4.01 %
$N = 5$	1143.43	28.56	2.49 %
$N = 6$	2274.13	38.84	1.70 %

Table4: Calculation time for the reduced and ODE models

By analyzing the difference provoked by the reduced equations it can be said that it is acceptable taking into account the tradeoff introduced by the great reduction in calculation time. This saving in time makes it possible the implementation of an identification and/or optimization process in a reasonable time with the aim of maximizing the output power of the energy harvesting device.

5. CONCLUSIONS

This paper presented a nonlinear mathematical formulation for inextensional Bernoulli-Euler beams with (unimorph or bimorph) piezoelectric sheets working in d_{31} or d_{33} mode that combines the most relevant contributions of the literature to this problem: (i) geometric nonlinearity induced by large displacements, (ii) material nonlinearities coming from ferroelastic hysteresis and (iii) quadratic non-linear viscous damping.

The final analytical model yields a total set of $N+1$ ordinary differential equations for the first N modes and for the voltage output of the piezoelectric sheet. However, the direct solution of this ordinary nonlinear differential system of N equations is computationally costly. As an alternative, a reduced algebraic system of $2(N+1)$ algebraic equations is proposed which was obtained by using the method of averaging. The main advantage of this reduced system is that it makes more suitable and computationally economical for the implementation of a parameter identification process.

Additionally, it is demonstrated that the linear formulation overestimates the generated voltage in a resonance condition and this effect is larger for a cantilever beam in a d_{31} generation mode. In the same sense, the contribution of each nonlinear parameter is carefully analyzed for cantilever beams, showing the importance of nonlinear analysis in this type of problems.

Several numerical and experimental tests were conducted to test the validity of the assumptions: an MFC piezoelectric cantilever beam in d_{33} and d_{31} mode and a multimodal system with an MFC in d_{33} mode. After performing an identification process using the proposed analytical model to obtain the linear and nonlinear coefficients, the reduced algebraic system is validated against numerical and experimental data.

ACKNOWLEDGMENTS

The authors wish to thank CONICET, ANPCyT, UNS and Secretaría de Ciencia y Tecnología UTN-FRBB.

APPENDIX A: COEFFICIENTS

$$M_i = 1 \quad , \quad C_i = 2\xi_i\omega_i \quad , \quad K_i = {\omega_i}^2$$

$$C_{nijk} = 2\xi_{ni}\omega_i \int_{L_1}^{L_1+L_2} \phi_i\phi_j\phi_k sign(\phi_j)dx$$

$$K_{nijk} = EI_n \int_{L_1}^{L_1+L_2} \phi_i\left({\phi_j}'''{\phi_k}''' + {\phi_j}''{\phi_k}^{IV}\right) sign({\phi_j}'')dx$$

$$K_{Gijkl} = EI\int_0^L \phi_i\left(\phi_j''\phi_k''\phi_l'' + 4\phi_j'\phi_k''\phi_l''' + \phi_j'\phi_k'\phi_l^{IV}\right)dx$$

$$= EI_{1,3}\left(\int_0^{L_1}(\ldots)dx + \int_{L_1+L_2}^{L}(\ldots)dx\right) + EI_2\int_{L_1}^{L_1+L_2}(\ldots)dx$$

$$\theta_i = \int_{L_1}^{L_1+L_2}\phi_i J_p(x)''dx$$

$$\theta_{nij} = \int_{L_1}^{L_1+L_2} J_{pn}(x)\phi_i\phi_j^{IV}sign(\phi_j'')dx$$

$$\theta_{Gijk} = \int_{L_1}^{L_1+L_2}\phi_i\left(J_p(x)'\phi_j'\phi_k'' + \frac{1}{2}J_p(x)''\phi_j'\phi_k'\right)dx$$

$$M_{ai} = \rho A\int_0^L \phi_i dx = \rho A_{1,3}\left(\int_0^{L_1}\phi_i dx + \int_{L_1+L_2}^{L}\phi_i dx\right) + \rho A_2\int_{L_1}^{L_1+L_2}\phi_i dx$$

$$\psi_i = \gamma J_p\int_{L_1}^{L_1+L_2}\phi_i''dx$$

$$\psi_{nij} = \gamma J_{pn}\int_{L_1}^{L_1+L_2}\phi_i''\phi_j''sign(\phi_j'')dx$$

$$\psi_{Gijk} = \gamma J_p\int_{L_1}^{L_1+L_2}\left(\phi_i'\phi_j'\phi_k'' + \frac{1}{2}\phi_j'\phi_k'\phi_i''\right)dx$$

$$EI_{1,3} = \frac{1}{12}c_{11}^s b_s {h_s}^3$$

$$EI_2 = \frac{1}{3}\left[c_{11}^s b_s h_s\left(3a^2 - 3ah_s + {h_s}^2\right) + c_{11}^p b_p h_p\left(3a^2 + 3ah_p + {h_p}^2\right)\right]$$

$$EI_n = \frac{1}{2}c_{111}^p b_p h_p\left(4a^3 + 6a^2 h_p + 4a{h_p}^2 + {h_p}^3\right)$$

$$a = \frac{c_{11}^s b_s {h_s}^2 - c_{11}^p b_p {h_p}^2}{2\left(c_{11}^s b_s h_s + c_{11}^p b_p h_p\right)}$$

$$C_p = \frac{n\epsilon_{11}b_p h_p}{l_p}$$

$$\rho A_{1,3} = \rho_s A_s = \rho_s b_s h_s$$

$$\rho A_2 = \rho_s A_s + \rho_p A_p = \rho_s b_s h_s + \rho_p b_p h_p$$

$$m_t = \rho_s A_s L + \rho_p A_p L_2$$

$$J_p = \frac{1}{2}e_{33}n_f b_f\frac{h_f}{l_p}\left(2a + 2h_k + h_f\right)(1 - 2\alpha)$$

$$J_{pn} = \frac{1}{3} e_{311} n_f b_f \frac{h_f}{l_p} \left[3a^2 + 3a(h_f + 2h_k) + 3h_k(h_f + h_k) + {h_f}^2\right](1 - 2\alpha)$$

Where n_f is the total number of piezoelectric fibers, b_f is the width of each fiber, and h_f and h_k are the thickness of the fiber and the polyamide respectively, as can be observed in Figure 11. Parameter α is a correction empiric parameter introduced to take into account the non-uniformity of the electric field in the thickness of the fiber [31].

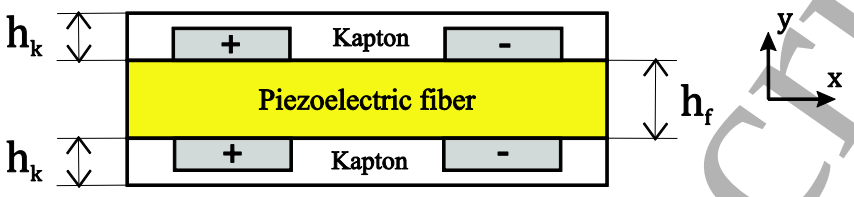

Figure11: Detail of a sheet of piezoelectric fibers of interdigitated electrodes for d_{33} mode generation.

For a d_{33} generation mode, the positions x_{i1} of function $f_H(x)$ related with Figure12, are given by:

$$\text{for} i = 1: \quad x_{11} = L_1, \qquad \text{for } i = k: \quad x_{k1} = x_{(k-1)6}$$

and for the rest:

$$x_{i2} = x_{i1} + \frac{w_p}{4} \quad , \quad x_{i3} = x_{i2} + l_p + \frac{w_p}{2}$$

$$x_{i4} = x_{i3} + \frac{w_p}{2} \quad , \quad x_{i5} = x_{i4} + l_p + \frac{w_p}{2} \quad , \quad x_{i6} = x_{i5} + \frac{w_p}{4}$$

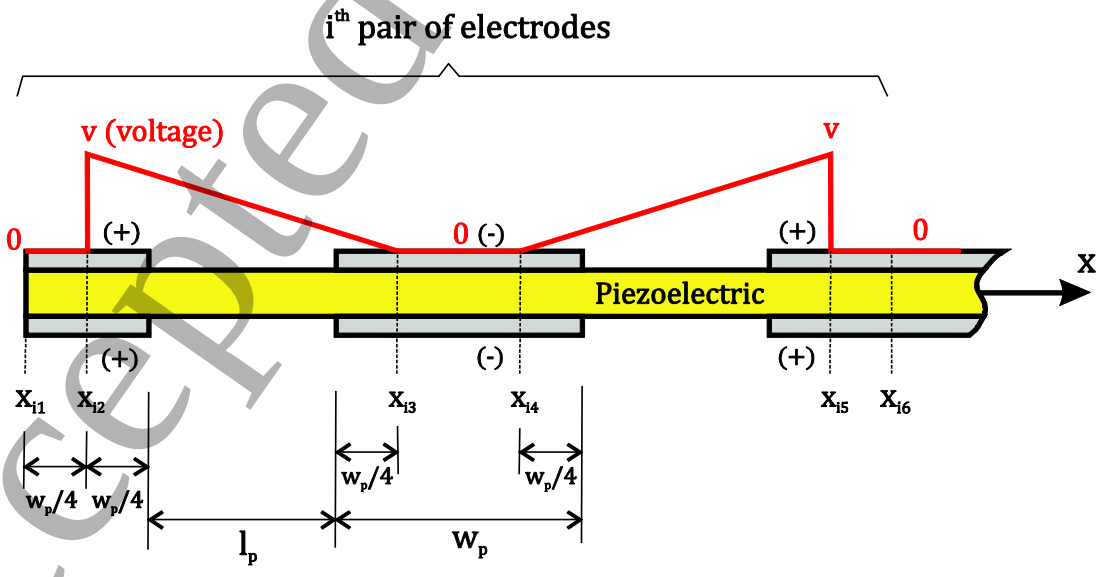

Figure12: Schematic representation of interdigitated electrodes for d_{33} generation mode.

For a d_{31} generation mode, the detail of the geometric parameters and the polarization of the electrodes over a sheet of piezoelectric fibers is shown in Figure 13.

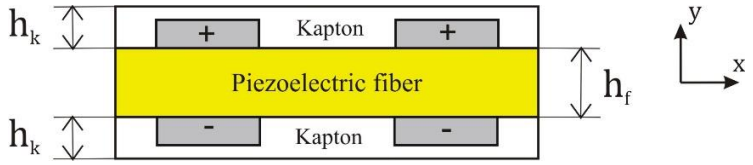

Figure13: Detail of a sheet of piezoelectric fibers of interdigitated electrodes for d_{31} mode generation.

The electric potential for a d_{31} generation mode over the length of the MFC is shown in Figure 14.

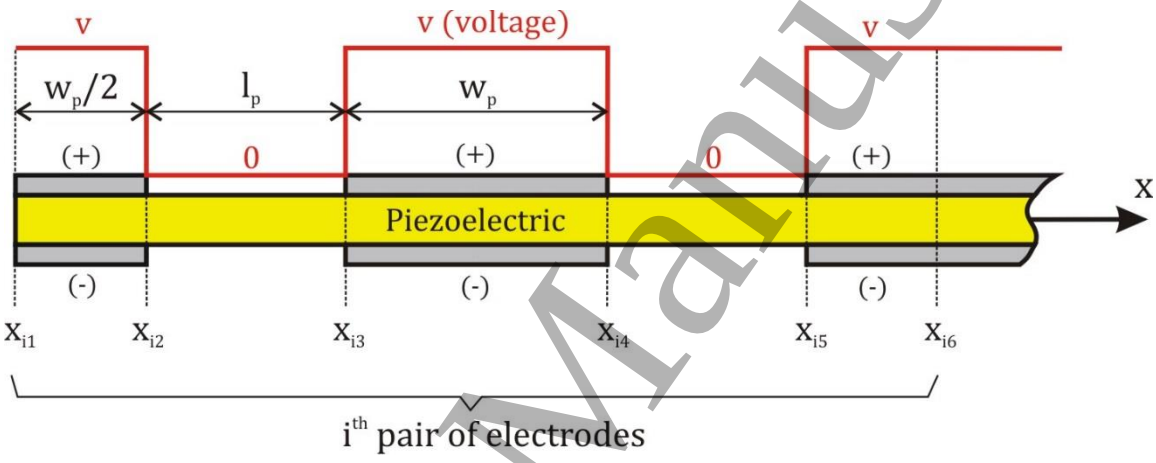

Figure 14: Schematic representation of interdigitated electrodes for d_{31} generation mode.

For a d_{31} generation mode, the positions x_{i1}, of function $f_H(x)$ related with Figure 14, are given by:

$$\text{for} i = 1: \quad x_{11} = L_1, \qquad \text{for } i = k: \quad x_{k1} = x_{(k-1)6}$$

and for the rest:

$$x_{i2} = x_{i1} + \frac{w_p}{2} \quad , \quad x_{i3} = x_{i2} + l_p$$

$$x_{i4} = x_{i3} + w_p \quad , \quad x_{i5} = x_{i4} + l_p \quad , \quad x_{i6} = x_{i5} + \frac{w_p}{2}$$

CONFLICT OF INTERESTS: The authors declare that they have no conflict of interest.

REFERENCES

[1] Meitzler A, Tiersten H, Warner A, Berlincourt D, Couqin G and Welsh III F 1988: Society)

[2] Gatti C D, Ramirez J M, Machado S P and Febbo M 2016 *J. Phys. Conf. Ser.* **773**

[3] Sadeqi S, Arzanpour S and Hajikolaei K H

[4] Zhu D, Tudor M J and Beeby S P 2010 *Measurement Science and Technology* **21** 022001

[5] Beeby S P, Tudor M J and White N 2006 *Measurement science and technology* **17** R175

[6] Erturk A and Inman D J 2011 *Piezoelectric energy harvesting*: John Wiley & Sons)

[7] Liu M and Gorman D 1995 *Computers & structures* **57** 277-85

[8] Stanton S C, Erturk A, Mann B P and Inman D J 2010 *Journal of Applied Physics***108** 074903

[9] Mak K H, Popov A A and McWilliam S 2012 *Journal of Sound and Vibration***331** 2602-23

[10] Joshi S P 1992 *Smart Mater. Struct.***1** 80

[11] Bertotti G and Mayergoyz I D 2006 *The science of hysteresis: Hysteresis in materials* vol 3: Gulf Professional Publishing)

[12] Damjanovic D 2006 *The science of hysteresis***3** 337-465

[13] Goldschmidtboeing F, Eichhorn C, Wischke M, Kroener M and Woias P 2011 In: *Proceedings of the 11th International Workshop on Micro and Nanotechnology for Power Generation and Energy Conversion Applications,* pp 114-7

[14] Aurelle N, Guyomar D, Richard C, Gonnard P and Eyraud L 1996 *Ultrasonics* **34** 187-91

[15] Albareda A, Gonnard P, Perrin V, Briot R and Guyomar D 2000 *IEEE transactions on ultrasonics, ferroelectrics, and frequency control* **47** 844-53

[16] Priya S, Viehland D, Carazo A V, Ryu J and Uchino K 2001 *Journal of applied physics* **90** 1469-79

[17] Leadenham S and Erturk A 2015 *Nonlinear Dynam.***79** 1727-43

[18] Gatti C, Ramirez J, Febbo M and Machado S 2018 *Journal of Mechanics of Materials and Structures* **13** 17-34

[19] Deuflhard P 2011 *Newton methods for nonlinear problems: affine invariance and adaptive algorithms* vol 35: Springer Science & Business Media)

[20] Beckert W and Kreher W S 2003 *Computational Materials Science* **26** 36-45

[21] Nelson L, Bowen C, Stevens R, Cain M and Stewart M 2003 In: *Smart Structures and Materials*: International Society for Optics and Photonics pp 556-67

[22] Rao S S 2007 *Vibration of continuous systems*: John Wiley & Sons)

[23] Nayfeh A H, Frank Pai P 2004 *Linear and Nonlinear Structural mechanics*: John Wiley & Sons)

[24] MEIROVITCH L AND PARKER R 2001 *APPLIED MECHANICS REVIEWS* **54** 100

[25] Joule J P 1847 *The London, Edinburgh, and Dublin Philosophical Magazine and Journal of Science* **30** 76-87

[26] Bandstra J 1983 *Journal of Vibration, Acoustics, Stress, and Reliability in Design* **105** 382-92

[27] Yang Y and Upadrashta D 2016 *Nonlinear Dynam.* **84** 2487-504

[28] Weaver Jr W, Timoshenko S P and Young D H 1990 *Vibration problems in engineering*: John Wiley & Sons)

[29] Stewartson K 1966: Wiley Online Library)

[30] Dormand J R and Prince P J 1980 *Journal of computational and applied mathematics* **6** 19-26

[31] Bilgen O, Erturk A and Inman D J 2010 *Journal of Vibration and Acoustics* **132** 051005